Structural Properties of Highly Doped Borazino Polyphenylenes Obtained through Condensation Reaction

Jacopo Dosso,[†,§] Davide Marinelli,[†,§] Nicola Demitri,[‡] and Davide Bonifazi*,[†]

[†]School of Chemistry, Cardiff University, Park Place, Cardiff CF10 3AT, U.K.

[‡]Elettra-Sincrotrone Trieste, S. S. 14 km 163.5 in Area Science Park, Basovizza 34149, Trieste, Italy

S *Supporting Information*

ABSTRACT: Here we describe the synthesis and spectroscopic and structural characterization of various borazine-doped polyphenylenes displaying high doping dosages (16−18%). Capitalizing on the condensation reaction approach, the desired products were formed using a mixture of *p*-phenylendiamine and aniline with BCl_3, followed by the addition of an aryl lithium derivative. The use of mesityl lithium (MesLi) yields strained multiborazine derivatives, which proved to be unstable in the presence of moisture. However, when xylyl lithium (XylLi) was used, chemically stable multiborazines were obtained, with oligomers showing molecular weight up to 10^4, corresponding to 16−18 monomer units. While the dimer, trimer, and tetramer could be isolated as pure products and their structure characterized by mass and NMR analysis, higher oligomers could only be isolated as mixtures of *B*-hydroxy-substituted derivatives and characterized by gel permeation chromatography. The structures of the dimer and trimer derivatives were confirmed by X-ray analysis, which nicely showed the presence of the two and three borazine rings spaced by one and two 1,4-aryl bridges, respectively. Notably, the trimer forms a porous crystalline clathrate. The peripheral xylyl and phenyl moieties of each molecule intramolecularly embrace each other through C−H and π−π stacking interactions. Steady-state UV−vis absorption characterization suggested that the molecules are UV absorbers, with the extinction coefficient linearly scaling with the degree of oligomerization. On the other hand, low-emission quantum yields were obtained for all derivatives (<7%), suggesting that high BN-doping dosages dramatically affect the emission properties of the doped polyphenylenes.

Enhancing doping dosage
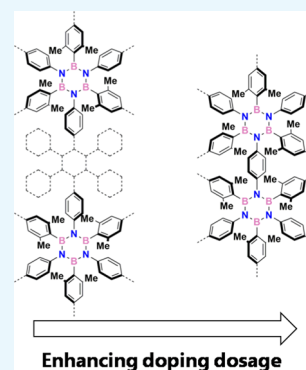
INTRODUCTION

In the last decade, the development of doping methods[1−3] to replace C=C bonds with B=N has proved to be one of the most promising synthetic approaches to tailor material properties both at the molecular and the nanoscale levels.[4−11] The interest is related to the peculiar characteristics of polar B=N bonds that,[10] being isoelectronic and isostructural to C=C bonds, allow the tuning of the optoelectronic properties[12−14] of polycyclic aromatic hydrocarbons and parent molecular graphenes without significant peripheral modifications of the molecular scaffold.[15−23] In this respect, a lot of efforts have been dedicated to the development of BN-doped polymeric[8,24−28] and dendrimeric[29] materials for applications in gas storage and separation,[30] optoelectronic devices,[19,21,22,27,31] self-assembly on surfaces,[32−34] and in the bottom-up synthesis of BN-doped nanographenes.[35,36] Although suffering from low stability toward hydrolysis,[37] El-Kaderi's porous polyborazino materials, prepared by condensation reaction and used to store H_2, are certainly the seminal examples in the field (Figure 1).[38,39] Inspired by Nagasawa's observations, who reported a moisture-stable *B*-trimesityl-*N*-triphenylborazine in 1965, and later by the group of Yamaguchi,[40] our group dedicated a lot of effort on the development of BN-doped polyphenylenes that are chemically and thermally stable.[29] In particular, we recently described the divergent synthesis of borazino-doped poly-

phenylenes, taking advantage of the decarbonylative Diels−Alder cycloaddition reaction between ethynyl and tetraphenylcyclopentadienone-borazine based precursors. Owing to the possibility of functionalizing the borazine core with different groups on the aryl substituents at the N and B atoms, we have prepared borazino-doped polyphenylenes featuring different doping dosages (ρ) and orientations (*o*). The ρ value is defined as the percentage of the aryl units that have been substituted with the borazine analogues, whereas the orientational parameter *o* defines the relative orientation between the doping borazine rings.[29] Detailed photophysical investigations showed that, increasing the ρ value to 6%, the strong fluorescent signal is progressively reduced. On the contrary, a negligible effect of the orientational *o* doping was observed. This observation suggested that high values of ρ accelerated the nonradiative deactivation of the singlet excited state through a possible combination of intersystem crossing, increased charge separation character of the excited state and vibrational relaxation.[29] To further expand and study the doping portfolio of polyphenylenes, we envisaged to prepare oligomeric BN-doped polyphenylenes featuring higher doping dosages. Conceptually, high ρ values can be achieved either by
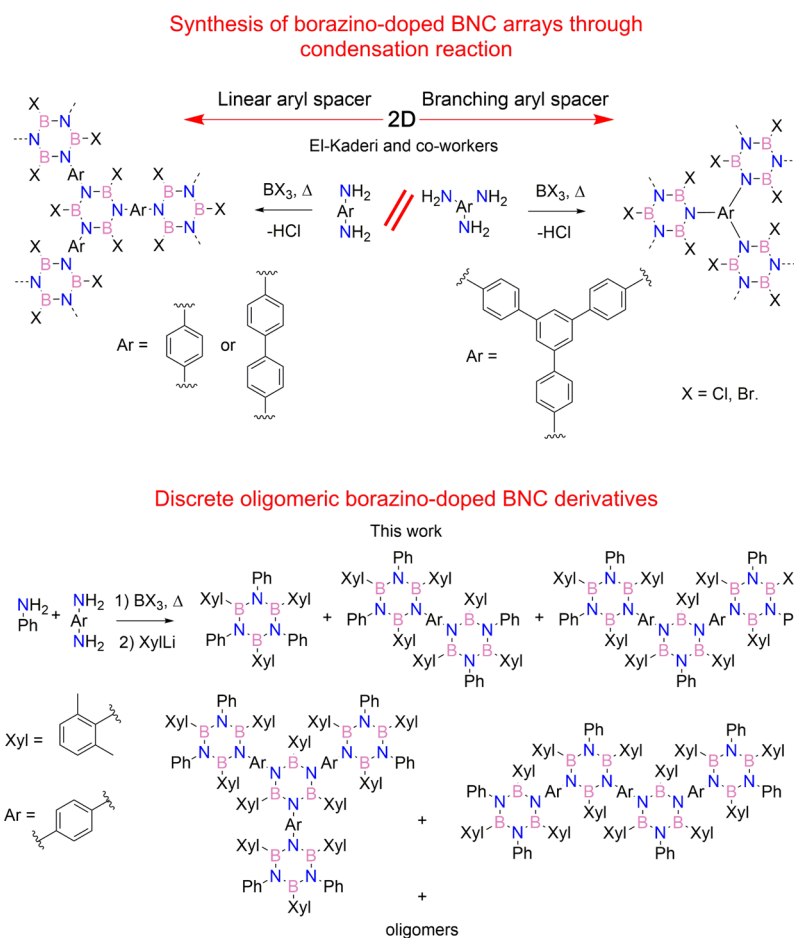
Figure 1. Synthetic strategy toward borazino-doped polymers and oligomers.

(i) replacing as many phenyl rings as possible with borazine rings or (ii) reducing the number of peripheral and core phenyl rings. Building on the latter approach, in this work we report on the synthesis of oligomeric borazines in which the hexaphenyl aryl bridge is replaced by 1,4-aryl linkers. Capitalizing on the condensation reaction between aniline and BCl₃ followed by the addition of an organolithium aryl derivative,[31,40] we have isolated BN-doped polyphenylenes with high ρ values (>16%). X-ray characterization confirmed the structures of the dimeric and trimeric borazines, whereas photophysical investigations confirmed the UV-absorption properties of the materials, as well as their doping-dependent emission properties.

■ RESULTS AND DISCUSSION

Building on El-Kaderi's approach,[38,39] we attempted the preparation of borazine-doped polyphenylenes using BCl₃ in the presence of a given mixture of aniline and *p*-phenylendiamine in refluxing toluene (Scheme 1a). A first attempt was carried out using a 4:1 mixture of aniline and *p*-phenylendiamine with BCl₃, followed by the addition of MesLi. Purification of the reaction mixture with SiO₂ gel column chromatography led to the isolation of **1^Mes** and **2^Mes** in 10 and 2% yield, respectively. When using a 2:1 ratio of aniline and *p*-phenylendiamine, high quantities of oligoborazinic fractions were obtained after addition of MesLi. Similarly, molecule **1^Mes** was isolated in 6% yield along with a fraction containing a mixture of oligomers. Separation of the oligomeric mixture via

recycling-gel permeation chromatography (Rec-GPC, Scheme 1b) led to the isolation of dimer **2^Mes** (5% yield) and a fraction containing trimer **3^Mes** (3% yield). The molecular structures of the oligomers were identified by NMR spectroscopy and mass spectrometry, the latter allowing the detection of the peak corresponding to the molecular ion (M⁺).

However, degradation of both **2^Mes** and in particular **3^Mes** was noticed upon exposure to ambient moisture condition, which made the isolation of pure **3^Mes** an impossible task using classical chromatographic techniques. Suitable crystals for X-ray analysis were obtained for molecule **2^Mes** (Figure 2) by slow evaporation of a CHCl₃ solution. As expected, the crystal structure shows the presence of two borazine rings, linked at the nitrogen atoms through a 1,4-aryl spacer. The molecular structure reveals a substantial deviation from the orthogonal arrangement of the aryl substituents and the borazine ring with an interplanar angle between 55.5 and 77.3°. Interestingly, the intra-annular distance values between B and N atoms within the borazine rings are between 1.441(1) and 1.448(1) Å, whereas the average internal NBN and BNB angles are 117.09(7)° and 122.31(7)°, respectively. The central BN core displays a significant structural deformation, with a r.m.s. deviation of 0.14 Å of the core BN atoms from the average plane.

When looking at the crystal structure of **2^Mes**, one can clearly notice that the 4-methyl group of Mes substituents at the bay position undergoes steric clashes, forcing the two neighboring BN cores to accommodate on two parallel planes (interplanar distance of 0.14 Å), straining the dimeric derivative and

Scheme 1. (a) Condensation Route To Prepare Multiborazino Polyphenylenes. The Addition of BCl₃ was Performed at 80 °C to Increase the Solubility of *p*-Phenylendiamine in Toluene. (b) Rec-GPC Trace of the Crude Oligomeric Mixture after SiO₂ Gel Column Chromatography, Showing the Waste (Black), Recycle (Blue), and Collection (Red) Sequences. Inset: Zoom of the Chromatogram of the Fourth Cycle
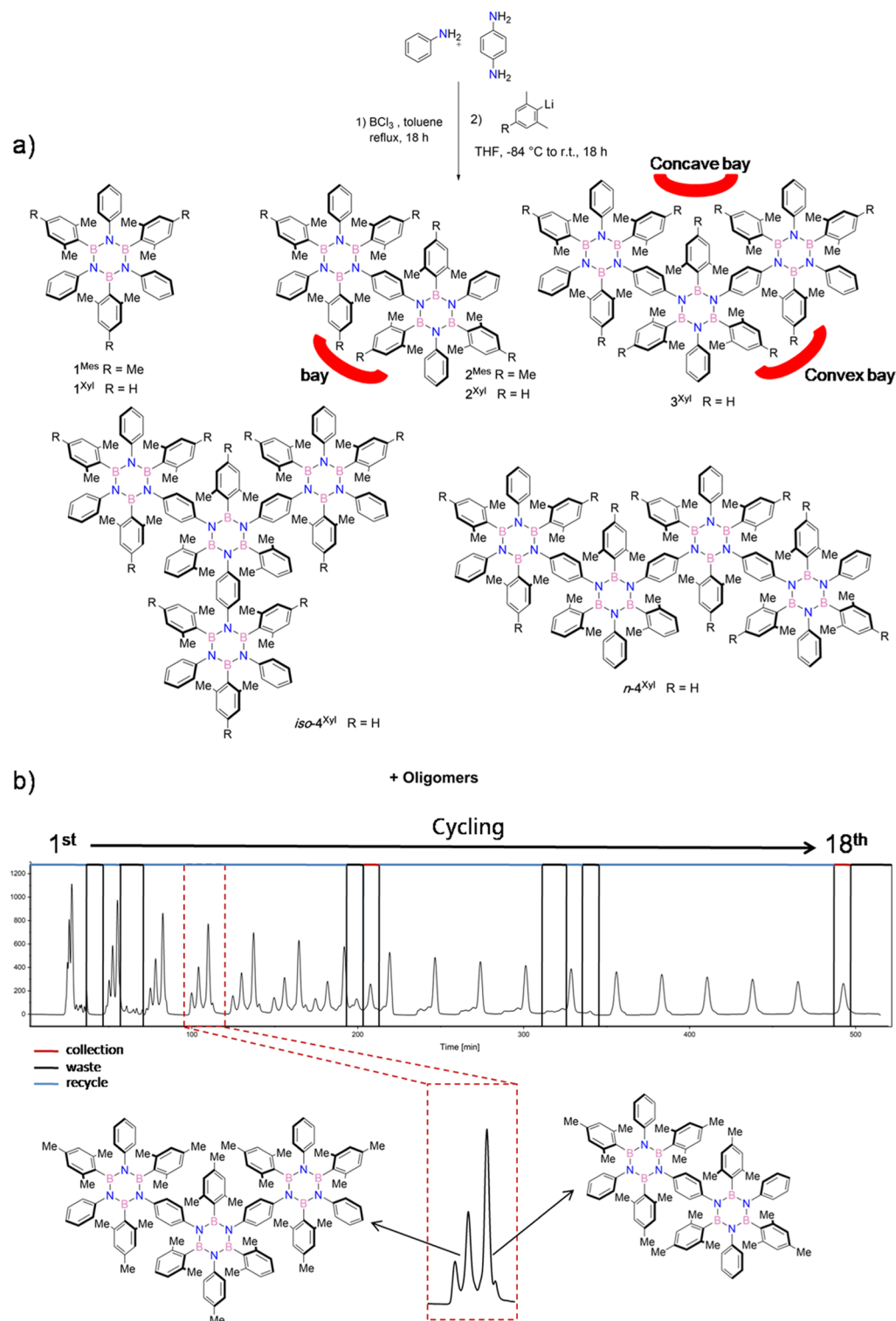
distorting the borazine ring. This results in a reduced steric protection of the boron atoms, which possibly leads to an increased susceptibility of the borazine cores toward hydrolysis. All together, these observations suggest that, if one wants to improve the stability of such oligomeric borazines toward hydrolysis, B-aryl moieties bearing no substituents at

the para position should be used. Therefore, we conjectured that addition of xylyl lithium (XylLi) would afford uncongested oligoborazines with a reduced strain content. Building on this idea, we reacted a 2:1 mixture of aniline and *p*-phenylendiamine with BCl₃ and quenched it with XylLi. Capitalizing on a combination of multiple chromatographic separations (see the
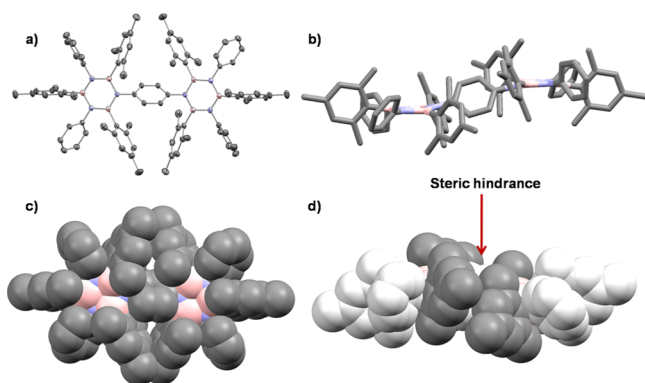
Figure 2. Front (a) and side (b) views of the X-ray structure of **2^{Mes}**, with the former depicted as ellipsoids of ASU contents (50% probability). Front (c) and side (d) views of the vdW representation, clearly depicting the steric clash between the Mes groups close to the bridging 1,4-aryl moiety. Space group: *Pbca*. B: pink, N: blue, C: gray. H atoms are omitted for clarity reasons.

Supporting Information), we could isolate **1^{Xyl}** (16% yield), **2^{Xyl}** (7% yield), **3^{Xyl}** (1% yield), **2^{XylOH}** (2% yield), **4^{Xyl}** (0.1% yield, probably as a mixture of iso and normal isomers, Scheme 1) along with an inseparable mixture of oligomeric products. The structural identity of the monodispersed fractions was first demonstrated by high-resolution mass spectrometry (HRMS), which confirmed the molecular mass for all oligomers (**1^{Xyl}**, $[C_{42}H_{43}B_3N_3]^+$ calcd, 622.3736; found, 622.3766; **2^{Xyl}**, $[C_{78}H_{78}B_6N_6]^+$ calcd, 1164.6846; found, 1164.6812; **3^{Xyl}**, $[C_{114}H_{114}B_9N_9]^+$ calcd, 1708.0035; found, 1707.9987; **2^{XylOH}**, $[C_{70}H_{70}B_6N_6O]^+$ calcd, 1076.6169; found, 1076.6207; and **4^{Xyl}**, $[C_{150}H_{150}B_{12}N_{12}]^+$ calcd, 2251.3223; found, 2251.3375). As the mixture of higher oligomers could not be separated, the product was analyzed using size exclusion chromatography calibrated on a poly(methylmethacrylate) standard (Figures S31 and S32). GPC analysis suggested that the fraction is mainly composed by oligomers displaying MW up to 10^4 Da, scoring an average molecular weight of 1900 Da and a dispersity of 1.97. The ^{11}B NMR spectrum displayed a peak centered at 37.5 ppm (diagnostic for borazine core) together with a low-intensity resonance at 25.2 ppm, typical of a boron specie linked to an oxygen atom. Considering that the IR spectrum of these oligomers closely resembles that of **2^{XylOH}** (see experimental part) with an intense OH-stretching absorption band centered at 3612 cm^{-1}, it is suggested that higher oligomers are mainly composed of hydroxylated species.

Suitable crystals for X-ray diffraction were obtained for **1^{Xyl}** (slow evaporation of CHCl$_3$, Figure 3), **2^{Xyl}**, **3^{Xyl}** (diffusion of pentane in a CHCl$_3$ solution, Figures 4 and 5), and **2^{XylOH}** (slow evaporation of a 1:1 CH$_2$Cl$_2$/petroleum ether mixture, Figures 6 and 7). Whereas the X-ray structure of **1^{Xyl}** closely resembles that obtained from the tri-*B*-mesityl derivatives previously reported by us (Figure 3),[31] the structure of bisborazine **2^{Xyl}** is less strained (Figure 4d) than that of its congener, **2^{Mes}**. Contrary to **2^{Mes}**, the absence of the 4-methyl groups lessens the steric hindrance between the B-aryl substituents, allowing the two borazine cores in **2^{Xyl}** to adopt a tilted conformation with an interplanar angle of 32° (Figure 4b). As a result, the boron atoms in the borazine core remain sterically shielded by the methyl groups, thus making derivative **2^{Xyl}** chemically stable toward hydrolysis, just as monomeric derivative **1^{Xyl}**.
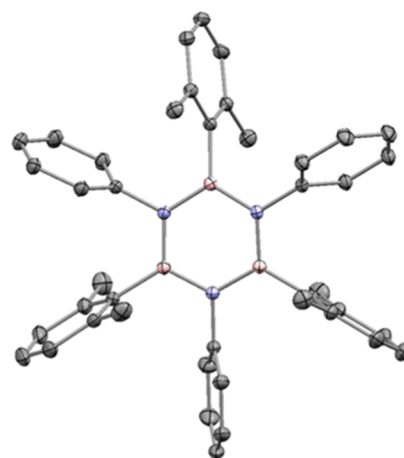

Figure 3. Front view of the X-ray structure of **1^{Xyl}** depicted as ellipsoids of ASU contents (50% probability), crystals obtained by slow evaporation of CHCl$_3$. Space group: *Cc*. B: pink, N: blue, C: gray. H atoms are omitted for clarity reasons.
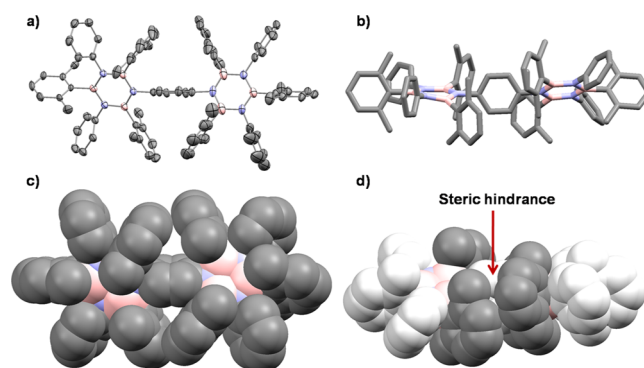

Figure 4. Front (a) and side (b) views of the X-ray structure of **2^{Xyl}**, with the former depicted as ellipsoids of ASU contents (50% probability). Front (c) and side (d) views of the vdW representation, depicting the steric clash between the xylyl groups at the bay position. Space group: *P$\bar{1}$*. B: pink, N: blue, C: gray. H atoms are omitted for clarity reasons.

Figure 5. Front (a) and side (b) views of the X-ray structure of **3^{Xyl}**, with the former depicted as ellipsoids of ASU contents (15% probability). Front (c) and side (d) views of the vdW representation, depicting the helices-type conformation adopted by the trimer as a consequence of the steric clash between the xylyl groups at the concave bay position. Space group: *P$\bar{3}$*. B: pink, N: blue, C: gray. H atoms are omitted for clarity reasons.
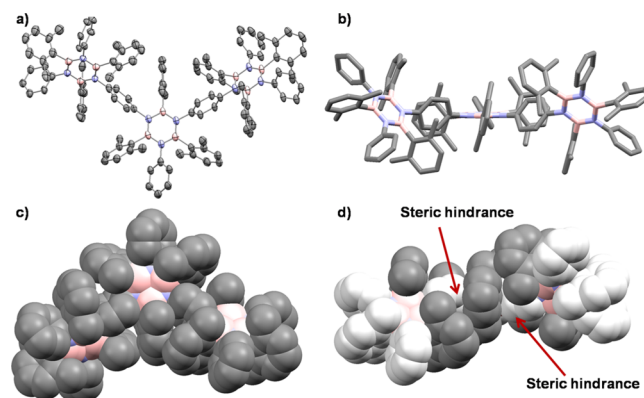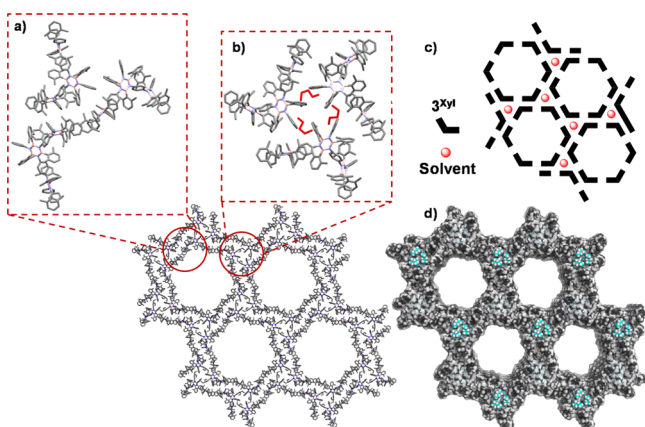
Figure 6. (a,b) Packing arrangement of the porous crystals obtained from 3^{Xyl}. Space group: $P\overline{3}$. B: pink, N: blue, C: gray. H atoms are omitted for clarity reasons. In red, the pentane molecules. (c) Schematic representation of molecules' arrangement in crystals. (d) vdW representation of the crystal packing with pores highlighted.
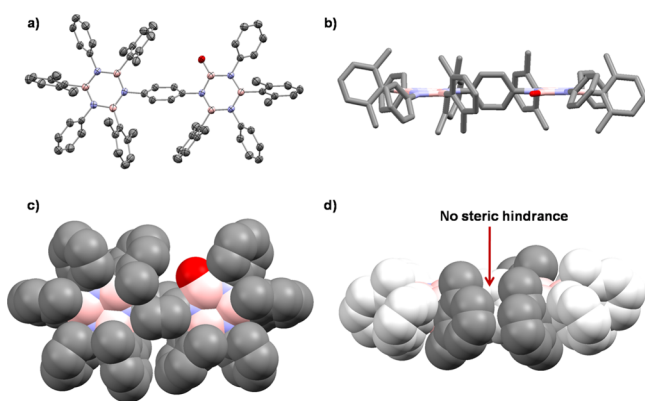

Figure 7. Front (a) and side (b) views of the X-ray structure of 2^{XylOH} in polymorph β with the former depicted as ellipsoids of ASU contents (50% probability). Front (c) and side (d) views of the vdW representation. Space group: $P2_1/c$. B: pink, N: blue, C: gray. H atoms are omitted for clarity reasons.

The same conformational pattern observed for dimer 2^{Xyl} was also noticed in the X-ray structure of 3^{Xyl} (Figure 5). In this case, three borazine units are linked through two 1,4-aryl spacers. If one considers the central borazine as the reference core, the two peripheral borazine rings adopt opposite tilted arrangements because of the steric hindrance between the xylyl substituents at the concave bay position, with interplanar angles of −53.0 and 53.5°, respectively. At the molecular level, the conformation develops into a helicene-type structure, with both enantiomers equally present in the crystal structure (Figure 5b−d). When looking at the crystal packing, it is apparent that molecule 3^{Xyl} forms a hierarchized hexagonal porous network at the solid state (Figure 6) with each pore surrounded by six molecules and displaying a diameter of 32 Å (Figure 6c). In the hierarchical structure, the molecules between different pores (Figure 6a,b) are held together by CH−π interactions through the interdigitation of peripheral aryl and phenyl groups (Figure 6a). Interestingly, three solvent molecules of pentane are also entrapped in the noncovalent hexagonal framework through CH−π interactions at each vertex.

As far as 2^{XylOH} is concerned, we found out that the molecule can crystallize in two different polymorphs α [unit cell: a = 18.861(4) Å; b = 22.390(4) Å; c = 14.820(3) Å] and β [a = 11.350(2) Å; b = 16.679(3) Å; c = 32.207(6) Å], forming rod- and plate-shape crystals, respectively. In both polymorphs, the crystal structure of 2^{XylOH} appears to be strain-free. Whereas in polymorph β the two borazine cores adopt an almost co-planar conformation (interplanar angle of 1.5°, Figure 8b), in the α crystals the BN rings form an interplanar
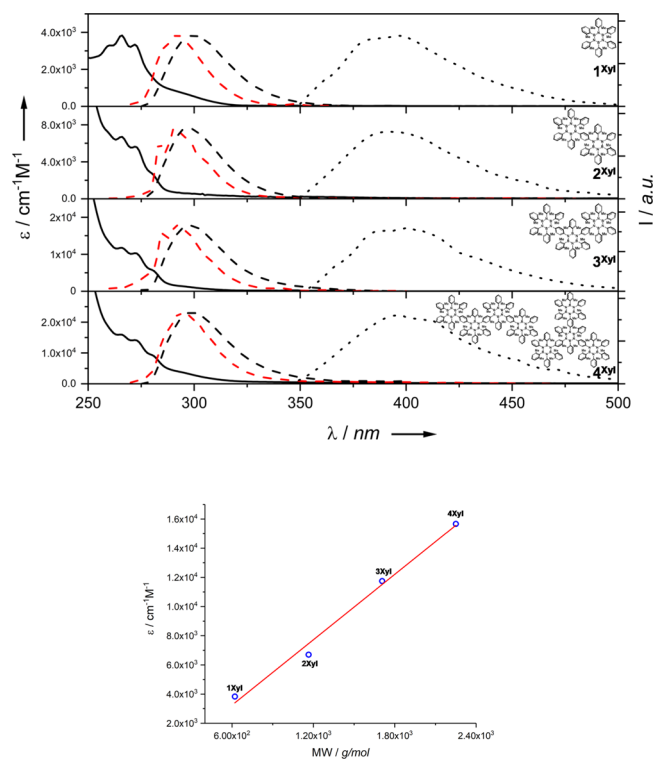

Figure 8. Above: Absorption (solid) and fluorescence (black dashed) in an aerated CH_2Cl_2 solution at rt. Fluorescence (red dashed) and phosphorescence (dotted) at 77 K in a 1:1 CH_2Cl_2/$CHCl_3$ glassy matrix of 1^{Xyl} (λ_{exc} = 265 nm), 2^{Xyl} (λ_{exc} = 265 nm), 3^{Xyl} (λ_{exc} = 267 nm), and 4^{Xyl} (λ_{exc} = 267 nm). Below: Correlation between MW and molar extinction coefficient at excitation wavelengths.

angle of 39° (Figures S4, S5 and S8). If one considers molecule 2^{Xyl} being stable under ambient conditions, it is unlikely that 2^{XylOH} could arise from direct hydrolysis of its arylated derivative. As we could isolate only derivatives bearing the B−OH group at the bay position, one can hypothesize that the hydrolysis reaction could occur at the B−Cl groups that, being sterically hindered, did not react with XylLi.

In order to study the effect of high doping dosages on the optoelectronic properties of borazine-polyphenylenes, the steady-state UV−vis absorption and emission properties of 1^{Xyl}, 2^{Xyl}, 3^{Xyl}, and 4^{Xyl} were studied (Figure 8, Table 1). As reported in the absorption spectra displayed in Figure 8a, all borazine-doped polyphenylenes absorb in the UV spectral region, with absorption maxima ranging from 260 to 280 nm. Although the extinction coefficients linearly scale with the molecular size of the oligomers when passing from 1^{Xyl} to 4^{Xyl} (Figure 8b), no significant bathochromic shifts are observed. These observations suggest that the absorption properties of these oligomers are additive, and that no significant π-conjugation occurs upon extension of the oligomers.

Table 1. Photophysical Properties of Oligoborazino Derivatives in CH_2Cl_2

	absorption					emission		
molecule	λ [nm] (ε, [M^{-1} cm^{-1}])[a]	$\lambda_{max,fl}$[a] [nm]	E_{opt}[b] [eV]	τ_{fl} [ns]	Φ_{fl}[c]	$\lambda_{max,ph}$[d] [nm]	τ_{ph}[d] [s]
1^{Xyl}	260 (3300)	300	4.31	1.24	0.02	383	1.11[e]
	266 (3831)						1.42 (76%)
	272 (3342)						0.37 (24%)
2^{Xyl}	266 (6702)	297	4.18	1.66	0.02	389	1.49[e]
	272 (5630)						1.70 (88%)
	280 (2755)						0.27 (12%)
3^{Xyl}	266 (11 747)	298	4.16	1.39	0.06	386	1.56[e]
	272 (10 300)						1.71 (88%)
	280 (5813)						0.14 (12%)
4^{Xyl}	266 (15 669)	299	4.15	1.36	0.07	393	1.46 (48%)
	272 (13 949)						0.26 (52%)
	280 (9100)						

[a]Recorded in an aerated CH_2Cl_2 solution at rt. [b]Calculated from the lowest energy crossing point between the normalized absorption and emission spectra (E_{opt} [eV] = $1240.5/\lambda_{cross}$ [nm]). [c]9,10-Diphenylanthracene was used as standard (0.97 in cyclohexane).[41] [d]Recorded at 77 K in a 1:1 $CH_2Cl_2/CHCl_3$ glassy matrix. [e]Monoexponential fitting.

Luminescence studies of air-equilibrated CH_2Cl_2 solutions of all borazine derivatives showed significant radiative UV emission profiles (λ_{max} = 266, 272, and 280 nm, Table 1) and very short lifetimes (τ_{fl} = 1.24−1.66 ns, Table 1) consistent with the presence of excited singlet radiative deactivation. No significant changes in the emission profiles were observed at 77 K for the fluorescence spectra. All solutions showed very low quantum yields (Φ_{em} = 2−7%; Table 1). These data are in line with those obtained with highly doped borazino-polyphenylenes, for which high BN dosages enhance the deactivation rate of the singlet excited state.[29] When cooled to 77 K, non-negligible phosphorescence emission has been also observed (Figure 8), showing double-peak emission profiles, also in line with borazino-polyphenylenes.[29] Representative phosphorescence lifetime measurements showed long-lasting emission profiles (τ_{ph} ca. ~1.11−1.56 s).

CONCLUSIONS

In conclusion, in this paper we have reported the synthesis, through a condensation reaction, of borazino-doped polyphenylene derivatives displaying high doping dosages (16−18%). The use of MesLi yielded strained derivatives, the latter revealing to be unstable in the presence of moisture. However, in the presence of XylLi, chemically stable derivatives were obtained, with a maximum degree of oligomerization of 16−18 units. Whereas the dimer, trimer, and tetramer could be isolated as pure products, higher oligomers could be only isolated as mixtures and characterized by GPC. The structures of the dimer and trimer molecules were confirmed by X-ray analysis, which nicely showed the presence of the two and three borazine rings spaced by one and two 1,4-aryl bridges, respectively. Notably, the trimer formed a porous crystalline clathrate with pentane at the solid state. Photophysical characterization suggested that the molecules are UV absorbers, with the excitation coefficient linearly scaling with the degree of oligomerization.

EXPERIMENTAL SECTION

Materials and Methods. Chemicals were purchased from Sigma-Aldrich, Acros Organics, TCI, Apollo Scientific, Alfa Aesar, and Fluorochem and were used as received. Solvents were purchased from Fisher Scientific, whereas deuterated

solvents from Eurisotop and Sigma-Aldrich. Tetrahydrofuran (THF) and toluene were dried on a Braun MB SPS-800 solvent purification system and further dried over activated 4 Å molecular sieves. 2-Bromomesitylene and 2-bromo-1,3-dimethylbenzene were dried over activated 4 Å molecular sieves. Aniline was distilled from CaH_2 under N_2 and stored away from light in an N_2 atmosphere. Aniline was left on CaH_2 overnight prior to distillation. Low-temperature baths were prepared using different solvent mixtures depending on the desired temperature: −84 °C with ethyl acetate/liq. N_2, and 0 °C with ice/H_2O. Anhydrous conditions were achieved by drying Schlenk tubes or two-neck flasks by flaming with a heat gun under vacuum and purging with nitrogen. The inert atmosphere was maintained using nitrogen-filled balloons equipped with a syringe and needle that was used to penetrate the silicon stoppers used to close the flasks' necks. Additions of liquid reagents were performed using plastic syringes. Degassing of solutions was performed using the freeze−pump−thaw (fpt) procedure: solutions were frozen using liquid nitrogen and kept under vacuum for 10′ before thawing. Molecular sieves (4 Å) were activated by heating at 165 °C under vacuum overnight and by further heating with heat gun under vacuum immediately before use. All reactions were performed in dry conditions and under inert atmosphere unless otherwise stated.

Synthesis of Borazines 1^{Mes} and 2^{Mes}. In a flame-dried 20 mL Schlenk-type flask, aniline (0.26 mL, 2.85 mmol), p-phenylendiamine (0.15 g, 1.40 mmol), and dry toluene (6 mL) were added. The mixture was heated at 80 °C under Ar and BCl_3 (1 M in heptane, 6.00 mL) added dropwise. The resulting suspension was stirred under refluxing conditions for 18 h, then cooled down to rt and subjected to 5 fpt cycles to remove the excess HCl. In parallel, to a solution of 2-bromomesitylene (0.71 mL, 4.70 mmol) in dry THF (15 mL), ^tBuLi (1.7 M in hexanes, 5.80 mL) was added dropwise at −84 °C. The solution was allowed to warm at 0 °C and stirred for 10 min. The degassed toluene suspension was thus transferred to the organometallic-containing THF solution at 0 °C and allowed to react for 18 h at rt. The final mixture was diluted with EtOAc (90 mL) and washed with water (3 × 100 mL) and brine (50 mL). The organic layer was dried over $MgSO_4$ and evaporated under reduced pressure. The products were purified by silica gel column chromatography (eluent: PE*/

CH$_2$Cl$_2$ 8:2) to afford **1^{Mes}** (36 mg, 6%) as a white powder. Additionally, a mixture of other products was obtained. These were separated by Rec-GPC using CHCl$_3$ as eluent to afford **2^{Mes}** (40 mg, 5%) as a white powder. *Petroleum ether.

1^{Mes} (Data According to Literature). ^{1}H NMR (400 MHz, CDCl$_3$): δ 6.84−6.70 (m, 15H), 6.33 (s, 6H), 2.23 (s, 18H), 1.97 (s, 9H). ^{13}C NMR (126 MHz, CD$_2$Cl$_2$): δ 146.42, 137.35, 136.17, 127.12, 126.81, 126.28, 124.27, 23.12, 21.15. ^{11}B NMR (128 MHz, CDCl$_3$): δ 37.02.

2^{Mes}. mp: >300 °C. ^{1}H NMR (400 MHz, CDCl$_3$): δ 6.69 (s, 20H), 6.39 (s, 8H), 6.29 (s, 4H), 6.12 (s, 4H), 2.15 (s, 12H), 2.10 (s, 12H), 1.95 (s, 6H), 1.89 (s, 24H). ^{13}C NMR (100 MHz, CDCl$_3$): δ 146.25, 141.97, 137.45, 137.33, 136.61, 136.10, 135.52, 127.24, 126.55, 126.39, 126.20, 125.83, 124.05, 22.87, 22.58, 21.30, 21.15. MALDI-TOF-HRMS: [M]$^+$ calcd for [C$_{84}$H$_{90}$B$_6$N$_6$]$^+$, 1248.7785; found, 1248.7786. IR not recorded because of instability of the molecule. Crystals suitable for X-ray diffraction were obtained from slow evaporation of CHCl$_3$.

Synthesis of Borazines 1^{Xyl}, 2^{Xyl}, 3^{Xyl}, and 4^{Xyl}. In a flame-dried 100 mL Schlenk-type flask, aniline (0.49 mL, 5.37 mmol), *p*-phenylendiamine (0.29 g, 2.68 mmol), and dry toluene (12 mL) were added. The mixture was heated at 80 °C under N$_2$ and BCl$_3$ (1 M in heptane, 11.5 mL) added dropwise. The reaction was cooled down to 0 °C and stirred for 10 min. The resulting suspension was heated under refluxing conditions for 18 h, cooled down to rt, and subjected to 5 fpt cycles to remove the excess HCl. In parallel, to a solution of 2-bromo-1,3-dimethylbenzene (2.16 mL, 16.08 mmol) in dry THF (40 mL), ^{n}BuLi (1.6 M in hexanes, 10.70 mL) was added dropwise at −84 °C. The solution was allowed to warm at 0 °C, and stirred for 10 min. The degassed toluene suspension was transferred to the organometal-containing THF solution at 0 °C and allowed to react for 18 h at rt. The final mixture was diluted with EtOAc (150 mL) and washed with water (2 × 100 mL) and brine (2 × 100 mL). The organic layer was dried over MgSO$_4$ and evaporated under reduced pressure. The solid residue was precipitated from cold MeOH and filtered. The resulting white solid was purified by silica gel column chromatography (eluent: PE/CH$_2$Cl$_2$ 7:3) to afford **1^{Xyl}** (182 mg, 16%) and **2^{Xyl}** (107 mg, 7%) as white powders. Additionally, three fractions composed by mixtures of products were obtained. The first two fractions were purified by Rec-GPC using CHCl$_3$ as eluent. Purification of the first fraction afforded **3^{Xyl}** (19 mg, 1%) and **2^{XylOH}** (22 mg, 2%) as white powders. Purification of the second fraction gave **4^{Xyl}** (iso and *n* isomers), which was further purified with preparative thin-layer chromatography (eluent: PE/CH$_2$Cl$_2$ 6:4) to give the desired product (2 mg, 0.1%). The third fraction was analyzed by GPC at Warwick University and resulted in a mixture of hydroxylated oligomers (see Section S4 of the Supporting Information for GPC analysis).

1^{Xyl}. mp: >300 °C. ^{1}H NMR (300 MHz, CDCl$_3$): δ 6.87−6.84 (m, 6H), 6.80−6.70 (m, 12H), 6.53 (d, *J* = 7.5 Hz, 6H) 2.30 (s, 18H). ^{13}C NMR (75 MHz, CDCl$_3$): δ 146.09, 137.50, 127.14, 126.98, 126.91, 125.39, 124.62, 23.29. ^{11}B NMR (160 MHz, CDCl$_3$): δ 36.43. IR (ATR) ν (cm^{-1}): 3061.03, 3008.95, 2947.23, 2916.37, 2854.65, 1595.13, 1489.05, 1427.32, 1355.96, 1288.45, 1072.42, 1026.13, 765.74, 748.38, 727.16, 696.30, 567.07, 528.50, 518.85. AP$^+$-HRMS: [M + H]$^+$ calcd for [C$_{42}$H$_{43}$B$_3$N$_3$]$^+$, 622.3736; found, 622.3766. Crystals suitable for X-ray diffraction were obtained from slow evaporation of CHCl$_3$.

2^{Xyl}. mp: >300 °C. ^{1}H NMR (500 MHz, CDCl$_3$): δ 6.85 (t, *J* = 6.5 Hz, 4H), 6.73 (s, 22H), 6.59−6.51 (m, 12H), 6.24 (s, 4H), 2.20 (s, 12H), 1.99 (s, 24H). ^{13}C NMR (126 MHz, CDCl$_3$): δ 145.94, 142.09, 137.57, 137.50, 127.09, 126.79, 126.65, 125.86, 125.63, 125.34, 124.40, 23.06, 22.94. ^{11}B NMR (160 MHz, CDCl$_3$): δ 37.13. IR (ATR) ν (cm^{-1}): 3057.17, 2943.37, 2914.44, 2858.51, 1595.13, 1489.05, 1452.4, 1352.10, 1288.45, 1070.49, 1018.41, 765.74, 698.23. MALDI-HRMS: [M]$^+$ calcd for [C$_{78}$H$_{78}$B$_6$N$_6$]$^+$, 1164.6846; found, 1164.6812. Crystals suitable for X-ray diffraction were obtained from slow diffusion of pentane in CHCl$_3$.

2^{XylOH}. mp: >300 °C. ^{1}H NMR (500 MHz, CDCl$_3$): δ 7.07 (t, *J* = 7.7 Hz, 1H), 7.00−6.96 (m, 2H), 6.79−6.78 (m, 4H), 6.76−6.64 (m, 16H), 6.60−6.56 (m, 2H), 6.53−6.48 (m, 10H) 6.43 (t, *J* = 8.1 Hz, 3H), 6.33 (d, *J* = 8.5 Hz, 1H), 3.49−3.17 (d, 1H, OH proton visible as double singlet because of exchange), 2.23 (s, 6H), 2.19 (s, 9H), 2.06 (br s, 6H), 1.98 (s, 6H), 1.90 (s, 3H). ^{13}C NMR (126 MHz, CDCl$_3$): δ 146.13, 146.04, 145.95, 144.32, 143.54, 142.87, 140.14, 139.55, 137.56, 137.52, 137.41, 137.25, 127.96, 127.48, 127.45, 127.19, 127.07, 126.97, 126.91, 126.87, 126.85, 126.80, 126.67, 125.89, 125.86, 125.56, 125.41, 125.38, 125.30, 125.10, 124.61, 124.56, 124.38, 23.17, 23.12, 22.92, 22.83. ^{11}B NMR (160 MHz, CDCl$_3$): δ 36.59, 26.27. IR (ATR) ν (cm^{-1}): 3601.10, 3059.10, 2916.37, 2854.65, 1678.07, 1597.06, 1508.33, 1490.97, 1452.40, 1425.40, 1354.03, 1307.74, 1213.23, 1163.08, 1122.57, 1074.35, 846.75, 765.74, 748.38, 729.09, 719.45, 696.30, 657.73, 607.58, 574.79, 526.57. ASAP$^+$-HRMS: [M]$^+$ calcd for [C$_{70}$H$_{70}$B$_6$N$_6$O]$^+$, 1076.6169; found, 1076.6207. Crystals suitable for X-ray diffraction were obtained from slow evaporation of petroleum ether CH$_2$Cl$_2$ mixture.

3^{Xyl}. mp: >300 °C. ^{1}H NMR (500 MHz, CDCl$_3$): δ 6.91 (t, *J* = 7.5 Hz, 1H), 6.83−6.75 (m, 7H), 6.70−6.68 (m, 21H), 6.61−6.60 (m, 3H), 6.57−6.52 (m, 12H), 6.50−6.47 (m, 8H), 6.13 (d, *J* = 8.7 Hz, 4H), 6.04 (d, *J* = 8.7 Hz, 4H), 2.16 (s, 12H), 1.95 (s, 12H), 1.94 (s, 12H), 1.80 (s, 12H), 1.62 (s, 6H). ^{13}C NMR (126 MHz, CDCl$_3$): δ 145.97, 145.94, 141.97, 141.92, 137.58, 137.55, 137.48, 127.13, 127.07, 126.76, 126.68, 126.63, 126.51, 126.39, 126.00, 125.64, 125.60, 125.51, 125.32, 124.39, 124.20, 23.07, 22.97, 22.95, 22.75, 22.52. ^{11}B NMR (160 MHz, CDCl$_3$): δ 39.21. IR (ATR) ν (cm^{-1}): 3039.81, 2916.37, 2854.65, 1597.06, 1425.40, 1352.10, 1301.95, 1288.45, 763.81, 698.23. MALDI-TOF-HRMS: [M]$^+$ calcd for [C$_{114}$H$_{114}$B$_9$N$_9$]$^+$, 1708.0035; found, 1707.9987. Crystals suitable for X-ray diffraction were obtained from slow diffusion of pentane in CHCl$_3$.

4^{Xyl}. mp: >300 °C. ^{1}H NMR (500 MHz, CD$_2$Cl$_2$): δ 6.93−6.44 (m, 69H), 6.21 (d, *J* = 8.7 Hz, 1H), 6.15−6.13 (m, 3H), 6.06−6.03 (m, 3H), 5.99 (d, *J* = 0.7 Hz, 2H), 2.26−2.12 (m, 18H), 1.97−1.95 (m, 18H), 1.81 (s, 9H), 1.80 (s, 3H), 1.62 (s, 6H), 1.52 (s, 18H). IR (ATR) ν (cm^{-1}): 3055.24, 2920.23, 2854.65, 1597.06, 1492.9, 1454.33, 1427.32, 1357.89, 1303.88. MALDI-TOF-HRMS: [M]$^+$ calcd for [C$_{150}$H$_{150}$B$_{12}$N$_{12}$]$^+$, 2251.3223; found, 2251.3375. ^{13}C not recorded because of the low amount of product obtained.

Oligomeric Fraction. IR (ATR) ν (cm^{-1}): 3612.67, 3057.17, 2945.30, 2916.37, 1597.06, 1490.97, 1355.96, 1307.74, 765.74, 698.23. ^{11}B NMR (160 MHz, CDCl$_3$): δ 37.53, 25.17. For GPC analysis see Section S4.

■ ASSOCIATED CONTENT

ⓢ Supporting Information

The Supporting Information is available free of charge on the ACS Publications website at DOI: 10.1021/acsomega.9b00830.

Synthetic protocols and spectroscopic characterizations (PDF)

Crystallographic data (CIF)
Crystallographic data (CIF)
Crystallographic data (CIF)
Crystallographic data (CIF)
Crystallographic data (CIF)
Crystallographic data (CIF)

■ AUTHOR INFORMATION

Corresponding Author

*E-mail: bonifazid@cardiff.ac.uk.

ORCID ⓘ

Nicola Demitri: 0000-0003-0288-3233
Davide Bonifazi: 0000-0001-5717-0121

Author Contributions

§J.D. and D.M. equally contributed to this work.

Notes

The authors declare no competing financial interest.

■ ACKNOWLEDGMENTS

■ REFERENCES

(1) Stępień, M.; Gońka, E.; Żyła, M.; Sprutta, N. Heterocyclic Nanographenes and Other Polycyclic Heteroaromatic Compounds: Synthetic Routes, Properties, and Applications. *Chem. Rev.* **2017**, *117*, 3479−3716.

(2) Hirai, M.; Tanaka, N.; Sakai, M.; Yamaguchi, S. Structurally Constrained Boron, Nitrogen, Silicon, and Phosphorus-Centered Polycyclic π-Conjugated Systems. *Chem. Rev.* **2019**, DOI: 10.1021/acs.chemrev.8b00637.

(3) Narita, A.; Wang, X.-Y.; Feng, X.; Müllen, K. New advances in nanographene chemistry. *Chem. Soc. Rev.* **2015**, *44*, 6616−6643.

(4) Wang, J.-Y.; Pei, J. BN-embedded aromatics for optoelectronic applications. *Chin. Chem. Lett.* **2016**, *27*, 1139−1146.

(5) Huang, J.; Li, Y. BN Embedded Polycyclic π-Conjugated Systems: Synthesis, Optoelectronic Properties, and Photovoltaic Applications. *Front. Chem.* **2018**, *6*, 341.

(6) Bosdet, M. J. D.; Piers, W. E. B−N as a C−C substitute in aromatic systems. *Can. J. Chem.* **2009**, *87*, 8−29.

(7) Campbell, P. G.; Marwitz, A. J. V.; Liu, S.-Y. Recent Advances in Azaborine Chemistry. *Angew. Chem., Int. Ed.* **2012**, *51*, 6074−6092.

(8) Helten, H. B=N Units as Part of Extended π-Conjugated Oligomers and Polymers. *Chem.—Eur. J.* **2016**, *22*, 12972−12982.

(9) Wang, X.-Y.; Wang, J. Y.; Pei, J. BN heterosuperbenzenes: Synthesis and properties. *Chem.—Eur. J.* **2015**, *21*, 3528−3539.

(10) Liu, Z.; Marder, T. B. B-N versus C-C: How similar are they? *Angew. Chem., Int. Ed.* **2008**, *47*, 242−244.

(11) Lorenzo-García, M. M.; Bonifazi, D. Renaissance of an Old Topic: From Borazines to BN-doped Nanographenes. *Chim. Int. J. Chem.* **2017**, *71*, 550−557.

(12) Karamanis, P.; Otero, N.; Pouchan, C. Unleashing the quadratic nonlinear optical responses of graphene by confining white-graphene (h -BN) sections in its framework. *J. Am. Chem. Soc.* **2014**, *136*, 7464−7473.

(13) Otero, N.; Karamanis, P.; El-Kelany, K. E.; Rérat, M.; Maschio, L.; Civalleri, B.; Kirtman, B. Exploring the linear optical properties of borazine (B₃N₃) doped graphenes. 0D flakes vs 2D sheets. *J. Phys. Chem. C* **2017**, *121*, 709−722.

(14) Otero, N.; Pouchan, C.; Karamanis, P. Quadratic nonlinear optical (NLO) properties of borazino (B₃N₃)-doped nanographenes. *J. Mater. Chem. C* **2017**, *5*, 8273−8287.

(15) Bosdet, M. J. D.; Piers, W. E.; Sorensen, T. S.; Parvez, M. 10a-Aza-10b-borapyrenes: Heterocyclic analogues of pyrene with internalized BN moieties. *Angew. Chem., Int. Ed.* **2007**, *46*, 4940−4943.

(16) Jaska, C. A.; Bosdet, M. J. D.; Parvez, M.; Sorensen, T. S.; Emslie, D. J. H.; Piers, W. E. Triphenylene Analogues with B₂N₂C₂ Cores: Synthesis, Structure, Redox Behavior, and Photophysical Properties. *J. Am. Chem. Soc.* **2006**, *128*, 10885−10896.

(17) Wang, X.-Y.; Zhuang, F.-D.; Wang, R.-B.; Wang, X.-C.; Cao, X.-Y.; Wang, J.-Y.; Pei, J. A straightforward strategy toward large BN-embedded π-systems: Synthesis, structure, and optoelectronic properties of extended BN heterosuperbenzenes. *J. Am. Chem. Soc.* **2014**, *136*, 3764−3767.

(18) Yang, D.-T.; Nakamura, T.; He, Z.; Wang, X.; Wakamiya, A.; Peng, T.; Wang, S. Doping Polycyclic Arenes with Nitrogen-Boron-Nitrogen (NBN) Units. *Org. Lett.* **2018**, *20*, 6741−6745.

(19) Hatakeyama, T.; Shiren, K.; Nakajima, K.; Nomura, S.; Nakatsuka, S.; Kinoshita, K.; Ni, J.; Ono, Y.; Ikuta, T. Ultrapure Blue Thermally Activated Delayed Fluorescence Molecules: Efficient HOMO-LUMO Separation by the Multiple Resonance Effect. *Adv. Mater.* **2016**, *28*, 2777−2781.

(20) Wang, X.-Y.; Zhuang, F.-D.; Wang, J.-Y.; Pei, J. Incorporation of polycyclic azaborine compounds into polythiophene-type conjugated polymers for organic field-effect transistors. *Chem. Commun.* **2015**, *51*, 17532−17535.

(21) Nakatsuka, S.; Yasuda, N.; Hatakeyama, T. Four-Step Synthesis of B₂N₂-Embedded Corannulene. *J. Am. Chem. Soc.* **2018**, *140*, 13562−13565.

(22) Hatakeyama, T.; Hashimoto, S.; Oba, T.; Nakamura, M. Azaboradibenzo[6]helicene: Carrier inversion induced by helical homochirality. *J. Am. Chem. Soc.* **2012**, *134*, 19600−19603.

(23) Bonifazi, D.; Fasano, F.; Lorenzo-garcia, M. M.; Marinelli, D.; Oubaha, H.; Tasseroul, J. Boron−nitrogen doped carbon scaffolding: organic chemistry, self-assembly and materials applications of borazine and its derivatives. *Chem. Commun.* **2015**, *51*, 15222−15236.

(24) Lorenz, T.; Crumbach, M.; Eckert, T.; Lik, A.; Helten, H. Poly (p -phenylene iminoborane): A Boron−Nitrogen Analogue of Poly (p -phenylene vinylene). *Angew. Chem., Int. Ed.* **2017**, *56*, 2780−2784.

(25) Resendiz-Lara, D. A.; Stubbs, N. E.; Arz, M. I.; Pridmore, N. E.; Sparkes, H. A.; Manners, I. Boron-nitrogen main chain analogues of polystyrene: Poly(B -aryl) aminoboranes via catalytic dehydrocoupling. *Chem. Commun.* **2017**, *53*, 11701−11704.

(26) Staubitz, A.; Sloan, M. E.; Robertson, A. P.; Friedrich, A.; Schneider, S.; Gates, P. J.; Schmedt auf der Günne, J.; Manners, I. Catalytic Dehydrocoupling/Dehydrogenation of N -Methylamine-Borane and Ammonia-Borane: Synthesis and Characterization of High Molecular Weight Polyaminoboranes. *J. Am. Chem. Soc.* **2010**, *132*, 13332−13345.

(27) Staubitz, A.; Presa Soto, A.; Manners, I. Iridium-catalyzed dehydrocoupling of primary amine-borane adducts: A route to high molecular weight polyaminoboranes, boron-nitrogen analogues of polyolefins. *Angew. Chem., Int. Ed.* **2008**, *47*, 6212−6215.

(28) Riensch, N. A.; Deniz, A.; Kühl, S.; Müller, L.; Adams, A.; Pich, A.; Helten, H. Borazine-based inorganic-organic hybrid cyclomatrix microspheres by silicon/boron exchange precipitation polycondensation. *Polym. Chem.* **2017**, *8*, 5264−5268.

(29) Marinelli, D.; Fasano, F.; Najjari, B.; Demitri, N.; Bonifazi, D. Borazino-Doped Polyphenylenes. *J. Am. Chem. Soc.* **2017**, *139*, 5503−5519.

(30) Jackson, K. T.; Reich, T. E.; El-Kaderi, H. M. Targeted synthesis of a porous borazine-linked covalent organic framework. *Chem. Commun.* **2012**, *48*, 8823−8825.

(31) Kervyn, S.; Fenwick, O.; Di Stasio, F.; Shin, Y. S.; Wouters, J.; Accorsi, G.; Osella, S.; Beljonne, D.; Cacialli, F.; Bonifazi, D. Polymorphism, fluorescence, and optoelectronic properties of a borazine derivative. *Chem.—Eur. J.* **2013**, *19*, 7771−7779.

(32) Kalashnyk, N.; Nagaswaran, P. G.; Kervyn, S.; Riello, M.; Moreton, B.; Jones, T. S.; De Vita, A.; Bonifazi, D.; Costantini, G. Self-assembly of decoupled borazines on metal surfaces: the role of the peripheral groups. *Chem.—Eur. J.* **2014**, *20*, 11856−11862.

(33) Kervyn, S.; Kalashnyk, N.; Riello, M.; Moreton, B.; Tasseroul, J.; Wouters, J.; Jones, T. S.; De Vita, A.; Costantini, G.; Bonifazi, D. "Magic" surface clustering of borazines driven by repulsive intermolecular forces. *Angew. Chem., Int. Ed.* **2013**, *52*, 7410−7414.

(34) Schwarz, M.; Garnica, M.; Fasano, F.; Demitri, N.; Bonifazi, D.; Auwärter, W. BN-Patterning of Metallic Substrates through Metal Coordination of Decoupled Borazines. *Chem.—Eur. J.* **2018**, *24*, 9565−9571.

(35) Sánchez-Sánchez, C.; Brüller, S.; Sachdev, H.; Müllen, K.; Krieg, M.; Bettinger, H. F.; Nicolaï, A.; Meunier, V.; Talirz, L.; Fasel, R.; et al. On-Surface Synthesis of BN-Substituted Heteroaromatic Networks. *ACS Nano* **2015**, *9*, 9228−9235.

(36) Dosso, J.; Tasseroul, J.; Fasano, F.; Marinelli, D.; Biot, N.; Fermi, A.; Bonifazi, D. Synthesis and Optoelectronic Properties of Hexa-peri-hexabenzoborazinocoronene. *Angew. Chem., Int. Ed.* **2017**, *56*, 4483−4487.

(37) Nagasawa, K. Borazines Stable to Hydrolysis. *Inorg. Chem.* **1966**, *5*, 442−445.

(38) Reich, T. E.; Behera, S.; Jackson, K. T.; El-Kaderi, H. M.; Jena, P. Highly selective CO_2/CH_4 gas uptake by a halogen-decorated borazine-linked polymer. *J. Mater. Chem.* **2012**, *22*, 13524−13528.

(39) Reich, T. E.; Jackson, K. T.; Li, S.; Jena, P.; El-Kaderi, H. M. Synthesis and characterization of highly porous borazine-linked polymers and their performance in hydrogen storage application. *J. Mater. Chem.* **2011**, *21*, 10629−10632.

(40) Wakamiya, A.; Ide, T.; Yamaguchi, S. Toward π-conjugated molecule bundles: Synthesis of a series of B,B′,B″-trianthryl-N,N′,N″-triarylborazines and the bundle effects on their properties. *J. Am. Chem. Soc.* **2005**, *127*, 14859−14866.

(41) Suzuki, K.; Kobayashi, A.; Kaneko, S.; Takehira, K.; Yoshihara, T.; Ishida, H.; Shiina, Y.; Oishi, S.; Tobita, S. Reevaluation of absolute luminescence quantum yields of standard solutions using a spectrometer with an integrating sphere and a back-thinned CCD detector. *Phys. Chem. Chem. Phys.* **2009**, *11*, 9850−9860.